Received 9 November 2020; revised 2 December 2020; accepted 3 December 2020. Date of publication 13 January 2021; date of current version 3 February 2021.
Digital Object Identifier 10.1109/OJAP.2021.3051474

UCA-Based OAM Non-Orthogonal Multi-Mode Multiplexing

RUI CHEN [1,2] (Member, IEEE), RUNZHONG YAO [1] (Graduate Student Member, IEEE), WEN-XUAN LONG [1] (Graduate Student Member, IEEE), MARCO MORETTI [3] (Member, IEEE), AND JIANDONG LI [1] (Fellow, IEEE)

[1] State Key Laboratory of ISN, Xidian University, Xi'an 710071, China
[2] National Mobile Communications Research Laboratory, Southeast University, Nanjing 210018, China
[3] Dipartimento di Ingegneria dell'Informazione, University of Pisa, 56126 Pisa, Italy
CORRESPONDING AUTHOR: R. CHEN (e-mail: rchen@xidian.edu.cn)

This work was supported in part by the open research fund of National Mobile Communications Research Laboratory, Southeast University under Grant 2021D04, and in part by the Natural Science Foundation of Guangdong Province of China under Grant 2114050001307.

ABSTRACT Electromagnetic waves carrying orbital angular momentum (OAM) can improve the spectral efficiency of communication systems by multiplexing a number of OAM modes. However, since being not able to perform water-filling power allocation and adaptive modulation for each sub-channel like closed-loop multiple-input multiple-output (MIMO) systems, the traditional orthogonal multi-mode OAM multiplexing system usually has poor bit error rate (BER) performance due to the inherent large divergence angle of high-order orthogonal OAM beams. Therefore, in this article we propose a non-orthogonal OAM (NO-OAM) multi-mode multiplexing scheme based on uniform circular array (UCA), which regulates the divergence angles of all non-orthogonal OAM beams to be the same, circumventing the problem that large beam divergence of high-order orthogonal OAM modes results in low received signal-to-noise ratio (SNR) at the receive UCA with a fixed aperture. Mathematical analysis and numerical simulations show that in contrast to the existing uniform concentric circular array (UCCA) beam adjustment scheme, the proposed NO-OAM scheme has slightly better beam adjustment effect but with only one UCA. Moreover, in contrast to the traditional orthogonal OAM multi-mode transmission, the proposed NO-OAM multi-mode multiplexing scheme has asymptotically equivalent channel capacity and much lower BER.

INDEX TERMS Orbital angular momentum (OAM), non-orthogonal, multi-mode multiplexing, uniform circular array (UCA).

I. INTRODUCTION

With the increasing growth of emerging multimedia services, such as short-form video, high-definition (HD) video and virtual reality (VR), wireless applications require higher and higher data rate. To satisfy the requirement, more and more high frequency bands such as millimeter wave and terahertz bands are being licensed for 5G and beyond wireless systems [1]. Besides exploiting more frequency bandwidth, innovative techniques such as advanced coding and modulation, cognitive radio (CR) and massive multiple-input multiple-output (MIMO) have been explored. In essence, all these techniques are based on planar electromagnetic (EM) waves physically.

Since it was discovered in 1992 that vortex light beams can carry orbital angular momentum (OAM) [2], a lot of research has focused on vortex EM waves that carries OAM as well [3]–[20]. The phase front of a vortex EM wave rotates with azimuth exhibiting a helical structure $e^{j\ell\psi}$ in space, where ψ is the transverse azimuth and ℓ can be an integer or a fraction that is defined as the OAM mode number [20]. It is demonstrated in [4] that a non-integer radio OAM mode can be decomposed into a series superposition of

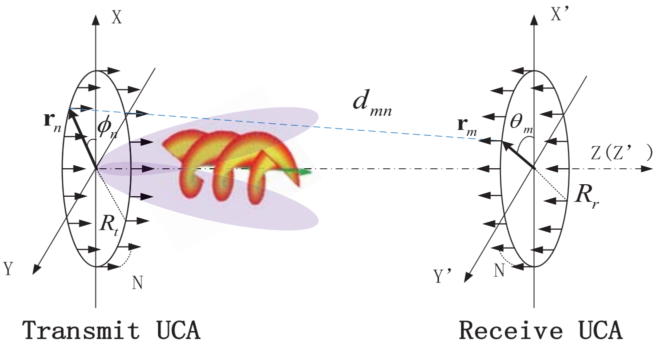

FIGURE 1. The line-of-sight OAM communication based on transmit and receive UCAs.

independent integer-order OAM modes. Due to the inherent orthogonality among different integer-order OAM modes, the OAM-based wireless communication enables a coaxial multiplexing approach, which utilizes a set of different integer-order OAM modes on the same frequency channel to achieve a high spectral efficiency (SE) [8], [11]–[18]. It is shown in [8] that multiplexing 8 OAM channels generated by spiral phase plates (SPPs) achieves 32Gbit/s in a wireless communication link at 28 GHz. Besides using SPP, the feasibility of utilizing uniform circular array (UCA) to generate and receive OAM waves has been verified in theory [5] and in practice [3], [6], [9] as shown in Fig. 1. After that, in order to further enhance the degree of freedom and increase the multiplexing gain of the line-of-sight (LoS) OAM communication systems, multiple concentric UCAs have been exploited in the transmitter and the receiver to achieve 100Gbit/s data rate [13].

However, there are still severe technical challenges for practical application of OAM wireless communications. One of the challenges is that orthogonal integer-order OAM beams are divergent, and the larger the OAM mode is, the larger the beam divergence angle becomes. Thus, different integer OAM modes result in large difference in the received signal energies. Especially, high-order integer OAM modes result in small received signal energy and low signal-to-noise ratio (SNR) at the receive UCA with a fixed aperture. Moreover, not like closed-loop MIMO systems being able to perform water-filling power allocation and adaptive modulation for each sub-channel with informed channel state information at the transmitter (CSIT), the orthogonal multi-mode OAM multiplexing system, which claims its advantage over MIMO system being low complexity due to no need of CSIT [12], [19], usually has poor bit error rate (BER) performance because the BER is dominated by the sub-channel with the lowest SNR, i.e., the sub-channel corresponding to the highest-order OAM mode.

To deal with the problem, several concentric circular arrays, i.e., uniform concentric circular arrays (UCCAs), are employed to adjust the orthogonal OAM beams' directivity, each array generating a beam carrying special OAM mode [21]. In spite of making sense for radar imaging, the beam adjustment with UCCA will reduce the spatial multiplexing gain for wireless communications. Therefore, in this article, we propose a non-orthogonal OAM (NO-OAM) multi-mode multiplexing scheme based on uniform circular array (UCA), which includes the generation, multiplexing transmission and reception of NO-OAM modes. The proposed generation method regulates the beam divergence angles of all NO-OAM modes to be the same with only one UCA, circumventing the problem of different OAM modes having large different receive SNRs. As the sacrifice, the receiver has to utilize successive interference cancellation (SIC) approach to cancel the inter-mode interference caused by the non-orthogonality between NO-OAM modes. Mathematical analysis and numerical simulations show that the proposed NO-OAM scheme has slightly better beam adjustment effect than the UCCA beam adjustment scheme [21], and has asymptotically equivalent channel capacity and much lower BER in contrast to the traditional orthogonal OAM multi-mode transmission.

Notations: Bold uppercase italic letter denotes a vector, bold lowercase letters denote column vectors, and bold uppercase letters denote matrices. $(\cdot)^T$, $(\cdot)^*$ and $(\cdot)^H$ denote transpose, conjugate and conjugate transpose, respectively. $\mathbf{I}$ is the identity matrix.

II. SYSTEM MODEL AND ORTHOGONAL OAM MULTIPLEXING

It is feasible and convenient to utilize the UCA to generate, steer and receive OAM beams [14], [19], [20]. In general, the UCA-based OAM communication system requires alignment of the transmit and receive arrays [7]–[9]. However, in case the transmit and receive UCAs are misaligned, beam steering could be adopted to eliminate the effect of the misalignment error and approaches the performance of an ideally aligned OAM channel [22]. Therefore, we consider an OAM communication system with aligned transmit and receive UCAs here. The transmit and receive UCAs both have N antennas and the radius of the transmitter and receiver are R_t and R_r, respectively, as shown in Fig. 1.

A. GENERATION OF ORTHOGONAL OAM MODES

The transmitter generates OAM beams by attaching incremental phases to N antennas of the UCA. The attached phase of the nth antenna element is $\ell_u\psi_n$, where $\psi_n = 2\pi(n-1)/N$ is the azimuthal angle of the nth antenna element, ℓ_u is the uth integer-order OAM mode. Thus, for the point $T(r,\varphi,\alpha)$ in space, the electric field vector can be expressed as [3]

$$\begin{aligned}\boldsymbol{E}_{\ell_u}(r,\varphi,\alpha) &= \frac{\beta_t}{4\pi}\sum_{n=1}^{N} e^{j\ell_u\psi_n}\int \frac{e^{jk|\boldsymbol{r}-\boldsymbol{r}_n'|}}{|\boldsymbol{r}-\boldsymbol{r}_n'|}dV_n' \\ &= \frac{\beta_t}{4\pi}\sum_{n=1}^{N} e^{j\ell_u\psi_n}\frac{e^{jk|\boldsymbol{r}-\boldsymbol{r}_n|}}{|\boldsymbol{r}-\boldsymbol{r}_n|} \\ &\approx \frac{\beta_t}{4\pi}\frac{e^{jkr}}{r}\sum_{n=1}^{N} e^{-j(\boldsymbol{k}\cdot\boldsymbol{r}_n-\ell_u\psi_n)}\end{aligned}$$

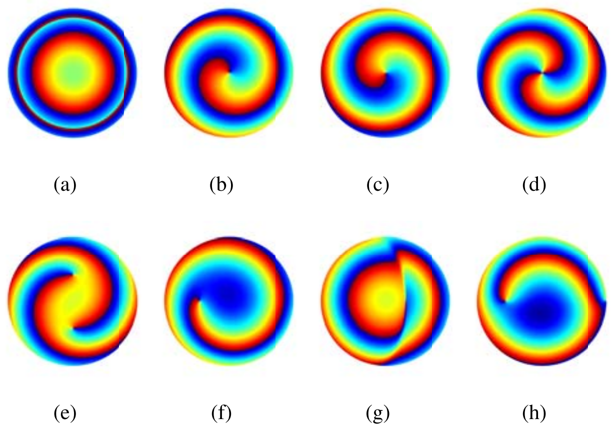

FIGURE 2. The rotational phase of an orthogonal OAM beam simulated with mode number: (a) $\ell_1 = 0$, (b) $\ell_2 = +1$, (c) $\ell_3 = -1$, (d) $\ell_4 = +2$ and the rotational phase of the NO-OAM beam simulated with mode number: (e) $\tilde{\ell_1}$, (f) $\tilde{\ell_2}$, (g) $\tilde{\ell_3}$, (h) $\tilde{\ell_4}$.

$$\begin{aligned} &\approx \frac{N\beta_t j^{-\ell_u} e^{jkr}}{4\pi r} J_{\ell_u}(kR_t \sin\alpha) e^{j\ell_u\varphi} \\ &= A_{\ell_u}(r, \alpha) e^{j\ell_u\varphi}, \end{aligned} \tag{1}$$

where the β_t models all the constants relative to each transmit antenna element, $j = \sqrt{-1}$ is the imaginary unit, $\boldsymbol{k}$ is the wave vector, $\boldsymbol{r}$ is the position vector of T. The far-field approximations are $|\boldsymbol{r} - \boldsymbol{r}_n| \approx r$ for amplitudes and $|\boldsymbol{r} - \boldsymbol{r}_n| \approx r - \hat{\boldsymbol{r}} \cdot \boldsymbol{r}_n$ for phases, where $\hat{\boldsymbol{r}}$ is the unit vector of $\boldsymbol{r}$, $\boldsymbol{r}_n = R_t(\hat{\boldsymbol{x}} \cos\phi_n + \hat{\boldsymbol{y}} \sin\phi_n)$, $\hat{\boldsymbol{x}}$ and $\hat{\boldsymbol{y}}$ are the unit vectors of x-axis and y-axis of the coordinate system at the transmitter respectively, and R_t is the radius of the transmitter, $J_{\ell_u}(\cdot)$ is ℓ_uth-order Bessel function of the first kind. According to (1), the generated phases of the orthogonal OAM beam with different topological charges are shown in Fig. 2 (a)–(d) and the orthogonal OAM beams radiation pattern with different OAM modes is shown in Fig. 3(a).

Considering any two OAM-carrying beams with integer OAM modes of ℓ_1 and ℓ_2, respectively,

$$\begin{cases} \boldsymbol{E}_{\ell_1}(r, \varphi, \alpha) = A_{\ell_1}(r, \alpha) e^{j\ell_1\varphi}, \\ \boldsymbol{E}_{\ell_2}(r, \varphi, \alpha) = A_{\ell_2}(r, \alpha) e^{j\ell_2\varphi}, \end{cases} \tag{2}$$

the inter-modal orthogonality can be simply proved by [12]

$$\int_0^{2\pi} \boldsymbol{E}_{\ell_1} \boldsymbol{E}^*_{\ell_2} d\varphi = \begin{cases} 0 & \text{if } \ell_1 \neq \ell_2, \\ A_{\ell_1} A^*_{\ell_2} & \text{if } \ell_1 = \ell_2, \end{cases} \tag{3}$$

which indicates that the OAM beams with different integer modes are orthogonal to each other, and can be used as independent carriers to send multiple spatially coaxial data streams on the same frequency at the same time without causing inter-channel interference (ICI) at the receiver.

B. ORTHOGONAL OAM MULTI-MODE MULTIPLEXING IN FREE SPACE

The radio propagation through the free-space channel leads to attenuation and phase rotation of the transmitted signal. This effect is modelled through multiplying the transmit signal by a complex constant h, whose value depends on the frequency and the distance d between the transmit and receive antennas. When the carrier frequency is determined, h can be expressed as [7]

$$h(d) = \beta \frac{\lambda}{4\pi d} \exp\left(-j\frac{2\pi d}{\lambda}\right), \tag{4}$$

where $\beta = \beta_r \beta_t$, β_r models all the constants relative to each receive antenna element, λ is the wavelength of the carrier. The distance between the n-th element of the transmit UCA and the m-th element of the receive UCA can be expressed as [22]

$$d_{m,n} = \left(R_t^2 + R_r^2 + D^2 - 2R_t R_r \cos(\phi_n - \theta_m)\right)^{\frac{1}{2}}, \tag{5}$$

where $\phi_n = \frac{2\pi}{N}(n-1) + \phi_0$, $\theta_m = \frac{2\pi}{N}(m-1) + \theta_0$, $n, m = 1, 2 \cdots N$, ϕ_0 and θ_0 are respectively the corresponding initial angles of the first reference antenna elements in the transmit and receive UCAs, for easier analysis, we assume $\phi_0 = 0$, $\theta_0 = 0$ here, D is the distance between the centers of the transmit and receive UCAs. Based on (4) and (5), the channel matrix of the considered LoS OAM system can be expressed as $\mathbf{H} = [h(d_{m,n})]_{N \times N}$. Since $d_{m,n}$ is the function of $|m - n|$, $\mathbf{H}$ is a circulant matrix, which can be diagonalized by the N-dimensional discrete Fourier transform (DFT) matrix $\mathbf{F}_N$ as $\mathbf{H} = \mathbf{F}_N^H \Lambda \mathbf{F}_N$, and $\Lambda = \text{diag}\{\lambda_1, \lambda_2, \ldots, \lambda_N\}$ is a diagonal matrix consisting of eigenvalues of $\mathbf{H}$.

The uth OAM mode corresponds to an independent transmit signal, denoted as $x(\ell_u)$. At the transmitter, the same $x(\ell_u)$ is loaded on all antenna elements with incremental phases to generate the uth mode OAM beam. After the transmitted signal on mode ℓ_u propagates to the receiver through the channel, the signal received by the mth element of the receive UCA can be expressed as

$$\begin{aligned} y_m(\ell_u) &= \frac{\beta}{2k} \sum_{n=1}^{N} \frac{e^{jk|\boldsymbol{r} - \boldsymbol{r}_n + \boldsymbol{r}_m|}}{|\boldsymbol{r} - \boldsymbol{r}_n + \boldsymbol{r}_m|} e^{j\ell_u\psi_n} x(\ell_u) + z_m \\ &= \frac{\beta}{2k} \sum_{n=1}^{N} \frac{e^{jkd_{m,n}}}{d_{m,n}} e^{j\ell_u\psi_n} x(\ell_u) + z_m \\ &= \sum_{n=1}^{N} h\big(d_{m,n}\big) e^{j\ell_u\psi_n} x(\ell_u) + z_m \\ &= \mathbf{h}_m \mathbf{f}^H(\ell_u) x(\ell_u) + z_m, \end{aligned} \tag{6}$$

where $k = \frac{2\pi}{\lambda}$, $\boldsymbol{r}_m = R_r(\hat{\boldsymbol{x}} \cos\theta_m + \hat{\boldsymbol{y}} \sin\theta_m)$, z_m is additive noise, $\mathbf{h}_m$ is the mth row of $\mathbf{H}$. Based on (6), the signal vector received by the receive UCA can be expressed as

$$\mathbf{y}(\ell_u) = \mathbf{H}\mathbf{f}^H(\ell_u) x(\ell_u) + \mathbf{z}, \tag{7}$$

where $\mathbf{y}(\ell_u) = [y_1(\ell_u), y_2(\ell_u), \ldots, y_N(\ell_u)]^T$, $\mathbf{f}(\ell_u) = \frac{1}{\sqrt{N}}[1, e^{-j\frac{2\pi\ell_u}{N}}, \ldots, e^{-j\frac{2\pi\ell_u(N-1)}{N}}]$, $\mathbf{z}$ is the noise vector. Considering $U(U \leq N)$ orthogonal OAM mode multiplexing, (7) can be expanded as

$$\mathbf{y} = \mathbf{H}\mathbf{F}_U^H \mathbf{x} + \mathbf{z}, \tag{8}$$

where $\mathbf{y} = \sum_{u=1}^{U} \mathbf{y}(\ell_u)$, $\mathbf{F}_U = [\mathbf{f}^H(\ell_1), \mathbf{f}^H(\ell_2), \ldots, \mathbf{f}^H(\ell_U)]^H$ is an $U \times N$ (partial) DFT matrix, $\mathbf{x} = [x(\ell_1), x(\ell_2),$

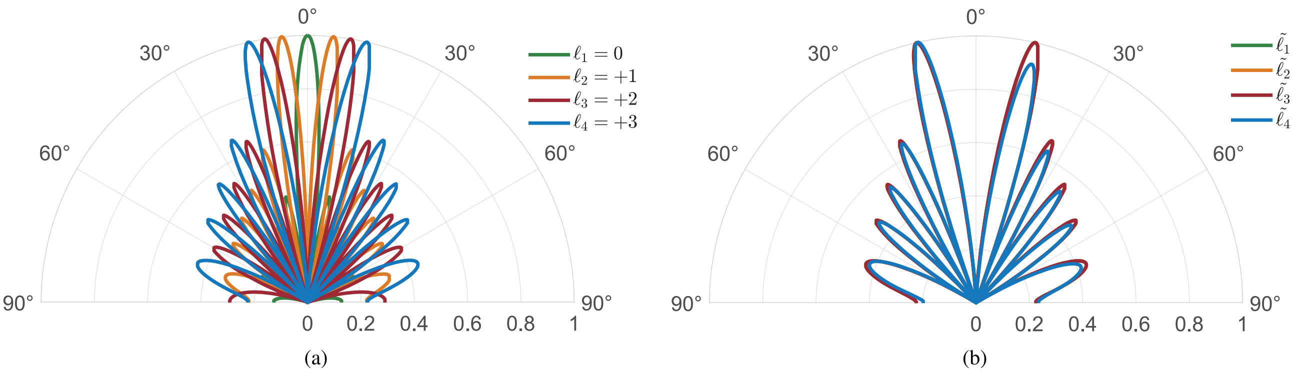

FIGURE 3. The beam radiation patterns generated by: (a) the orthogonal OAM scheme, (b) the proposed NO-OAM scheme at 9GHz, $R_t = R_r = 3\lambda$.

$, \ldots, x(\ell_U)]^T$. Then, the despiralized signal vector $\widehat{\mathbf{x}}$ takes the form

$$\begin{aligned}\widehat{\mathbf{x}} &= \mathbf{F}_U\Big(\mathbf{H}\mathbf{F}_U^H\mathbf{x} + \mathbf{z}\Big)\\ &= \Lambda_U\mathbf{x} + \widetilde{\mathbf{z}},\end{aligned} \tag{9}$$

where $\widehat{\mathbf{x}} = [\hat{x}(\ell_1), \hat{x}(\ell_2), \ldots, \hat{x}(\ell_U)]^T$, $\widetilde{\mathbf{z}} = \mathbf{F}_U\mathbf{z}$, $\Lambda_U = \mathrm{diag}\{\lambda_1, \lambda_2, \ldots, \lambda_U\}$ is the effective multi-mode OAM channel matrix whose complex diagonal elements are the U eigenvalues of $\mathbf{H}$. Thus, the channel capacity of orthogonal OAM multiplexing system is

$$C_{\mathrm{OAM}} = \sum_{u=1}^{U} \log_2\Big(1 + \frac{\rho}{U}|\lambda_u|^2\Big), \tag{10}$$

where ρ is the transmit SNR.

III. APPLICATION DILEMMA OF ORTHOGONAL OAM MULTIPLEXING AND EXISTING BEAM ADJUSTMENT

A. APPLICATION DILEMMA OF ORTHOGONAL OAM MULTI-MODE MULTIPLEXING

It can be seen from the Section II that the independent parallel multiple orthogonal OAM channels Λ_U have no ICI, which takes the form

$$\begin{aligned}\Lambda_U &= \mathbf{F}_U\mathbf{H}\mathbf{F}_U^H\\ &= \frac{\beta\lambda}{4\pi N}\mathrm{diag}\Bigg\{\sum_{m=1}^{N}\sum_{n=1}^{N}\frac{1}{d_{mn}}e^{-j\frac{2\pi}{\lambda}d_{mn}+j\frac{2\pi}{N}\ell_1(n-m)},\\ &\qquad \sum_{m=1}^{N}\sum_{n=1}^{N}\frac{1}{d_{mn}}e^{-j\frac{2\pi}{\lambda}d_{mn}+j\frac{2\pi}{N}\ell_2(n-m)}, \ldots,\\ &\qquad \sum_{m=1}^{N}\sum_{n=1}^{N}\frac{1}{d_{mn}}e^{-j\frac{2\pi}{\lambda}d_{mn}+j\frac{2\pi}{N}\ell_U(n-m)}\Bigg\}.\end{aligned} \tag{11}$$

When N is large enough and $D \gg R_t, R_r$, Λ_U can be approximately expressed as

$$\begin{aligned}\Lambda_U \approx \frac{N\beta\lambda}{4\pi D}e^{-j\frac{2\pi}{\lambda}D}\mathrm{diag}\Bigg\{(j)^{\ell_1}J_{\ell_1}\Big(\frac{4\pi R_t R_r}{\lambda D}\Big), (j)^{\ell_2}J_{\ell_2}\\ \times\Big(\frac{4\pi R_t R_r}{\lambda D}\Big), \ldots, (j)^{\ell_U}J_{\ell_U}\Big(\frac{4\pi R_t R_r}{\lambda D}\Big)\Bigg\}.\end{aligned} \tag{12}$$

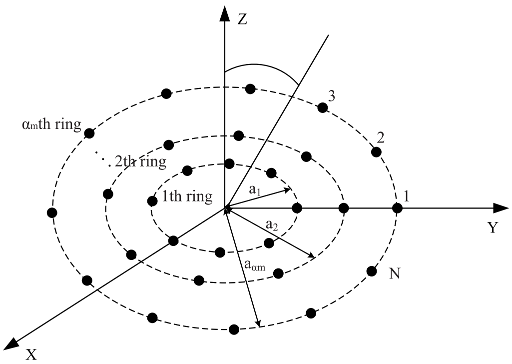

FIGURE 4. The UCCA for adjusting beam divergence angles of different orthogonal OAM modes in [21].

Due to $D \gg R_t, R_r$, $\frac{4\pi R_t R_r}{\lambda D}$ is a small value, and the larger the ℓ_u, the smaller the value of $J_{\ell_u}(\frac{4\pi R_t R_r}{\lambda D})$. This conclusion is consistent with the previous analysis that the larger the OAM mode is, the larger the divergence angle becomes, which can be seen from the Fig. 3 (a) apparently. Therefore, high-order and low-order integer OAM modes result in quite different received SNRs. Since not like closed-loop MIMO systems being able to perform water-filling power allocation and adaptive modulation for each sub-channel with CSIT, the orthogonal multi-mode OAM multiplexing transmission, which claims its advantage over MIMO system being low complexity due to no need of CSIT [12], [19], therefore has poor BER performance deteriorated by the higher-order OAM modes with the low received SNRs.

B. EXISTING ORTHOGONAL OAM BEAM ADJUSTMENT WITH UCCA

Since the angle of maximum gain reduces with the increasing aperture of the array [3], the direct idea is adopting large radius for high-order OAM modes and small radius for low-order OAM modes. The UCCA are proposed to achieve this concept in [21] as shown in Fig. 4, where a_{α_m} is the radius of the α_{m}th UCA in the UCCA, and the α_{m}th UCA is used to generate the mth mode OAM beam. The OAM beam divergence angle γ_G can be expressed as

$$\gamma_G = \arg\max_{\gamma}\left\{J_\alpha^2(ka\sin\gamma)\right\}. \quad (13)$$

Therefore, when the OAM mode and carrier frequency are determined, the relationship between γ_G and a can be determined. It is proposed in [21] that the position $t_{\max}$ with the maximum of $J_\alpha^2(t)$ for a given α can be approximately by curve fitting as

$$t_{\max}(\alpha) = 1.02\alpha + 1.874, \alpha > 0. \quad (14)$$

Thus, the radius of the UCA for generating a specified OAM beam divergence angle γ_G can be determined as [21]

$$a(\alpha) = \frac{1.02\alpha + 1.874}{k\sin\gamma_G}. \quad (15)$$

Therefore, the beam divergence angles of different orthogonal OAM modes are adjusted to be consistent, which is plotted in Fig. 5(a) for illustration.

IV. NON-ORTHOGONAL OAM MULTI-MODE MULTIPLEXING

A. GENERATION OF NON-ORTHOGONAL OAM SIGNALS

To deal with the application dilemma of orthogonal OAM multi-mode multiplexing, we propose a NO-OAM multi-mode multiplexing scheme. Compared with the orthogonal OAM scheme, the proposed NO-OAM scheme can adjust the beam divergence angles of all the modes to be consistent, thus equalizing the SNR of each OAM channel. Specifically, a NO-OAM mode is generated by the weighted superposition of integer-order OAM modes. We assume $p_{\ell_i,\tilde{\ell}_u}$ represents the weighting coefficient of the integer OAM mode ℓ_i in the superposed NO-OAM mode $\tilde{\ell}_u$. Then, the electric field vector of the point $T(r,\varphi,\alpha)$ in spherical coordinates in the direction of the NO-OAM beam can be expressed as

$$\begin{aligned}\boldsymbol{E}_{\tilde{\ell}_u}(r,\varphi,\alpha) &= \sum_{i=1}^{U}\boldsymbol{E}_{\ell_i}(r,\varphi,\alpha)p_{\ell_i,\tilde{\ell}_u}\\ &\approx \sum_{i=1}^{U}\left[\frac{\beta_t}{4\pi}\frac{e^{jkr}}{r}\sum_{n=1}^{N}e^{-j(\boldsymbol{k}\cdot\boldsymbol{r}_n-\ell_i\psi_n)}\right]p_{\ell_i,\tilde{\ell}_u}\\ &= \frac{\beta_t}{4\pi}\frac{e^{jkr}}{r}\sum_{n=1}^{N}\left[\sum_{i=1}^{U}e^{j\ell_i\psi_n}p_{\ell_i,\tilde{\ell}_u}\right]e^{-j\boldsymbol{k}\cdot\boldsymbol{r}_n}. \quad (16)\end{aligned}$$

Correspondingly, a $U\times U$ matrix $\mathbf{P} = [p_{\ell_i,\tilde{\ell}_u}]_{U\times U}$ can be constructed for generating the U mode multiplexed NO-OAM beams. Then, in contrast to the formulation of generating orthogonal OAM beams with $\mathbf{F}_U^H$ in (8), the generation of NO-OAM beams can be expressed in the similar matrix form as $\mathbf{F}_U^H\mathbf{P}$, and $\mathbf{P}$ is termed as the *NO-OAM generation matrix*. Since each NO-OAM mode is composed of a set of specific orthogonal modes, the NO-OAM modes are hardly orthogonal.

Then, we will design the NO-OAM generation matrix $\mathbf{P}$. Before proceeding further, we need to first introduce the following lemma, which will be used later.

Lemma 1: The effective OAM channel matrix Λ_U can be decomposed as

$$\Lambda_U = \mathbf{S}_L\mathbf{R}\mathbf{S}_R^H\mathbf{V}, \quad (17)$$

where $\mathbf{R}\in\mathbb{R}^{U\times U}$ is an upper triangular matrix whose diagonal elements are all equal to $\bar{\sigma}$, and $\bar{\sigma} = (\prod_{u=1}^{U}|\lambda_u|)^{\frac{1}{U}}$, $\mathbf{S}_L\in\mathbb{R}^{U\times U}$ and $\mathbf{S}_R\in\mathbb{R}^{U\times U}$ are unitary matrices, $\mathbf{V}\in\mathbb{C}^{U\times U}$ is a diagonal matrix whose elements are the phases of the diagonal elements of Λ_U.

Proof: According to [23], the implementation algorithm of geometric mean decomposition of Λ_U can be summarized as the following steps:

- Step 1: Decompose Λ_U as $\Lambda_U = \mathbf{W}\mathbf{V}$, where $\mathbf{W}\in\mathbb{R}^{U\times U}$ is a diagonal matrix, whose elements are the amplitudes of diagonal matrix Λ_U. Initialize $\mathbf{R}^{(1)} = \mathbf{W}$ and enter a loop.
- Step 2: In the ath $(1\le a\le (U-1))$ loop, first check the ith diagonal element of $\mathbf{R}^{(a)}$: if $\mathbf{R}^{(a)}(a,a)\ge\bar{\sigma}$, find a certain element $\mathbf{R}^{(a)}(b,b)(b>a)$ such that $\mathbf{R}^{(a)}(b,b)\le\bar{\sigma}$; Otherwise, find a certain element $\mathbf{R}^{(a)}(b,b)(b>a)$ such that $\mathbf{R}^{(a)}(b,b)\ge\bar{\sigma}$. Then, swap $\mathbf{R}^{(a)}(a+1,a+1)$ and $\mathbf{R}^{(a)}(b,b)$ by the corresponding permutation matrix $\mathbf{M}^{(a)}\in\mathbb{R}^{U\times U}$.
- Step 3: Construct two Givens matrices $\mathbf{G}_L^{(a)}\in\mathbb{R}^{U\times U}$ and $\mathbf{G}_R^{(a)}\in\mathbb{R}^{U\times U}$ by modifying the elements in $\mathbf{I}_U$ which lie at the intersection of rows a and $a+1$ and columns a and $a+1$. Focus on the relevant 2×2 submatrices of $\mathbf{G}_L^{(a)}$ and $\mathbf{G}_R^{(a)}$, the specific expression is as follows

$$\bar{\sigma}^{-1}\begin{bmatrix}c\delta_1 & s\delta_2\\ -s\delta_2 & c\delta_1\end{bmatrix}\begin{bmatrix}\delta_1 & 0\\ 0 & \delta_2\end{bmatrix}\begin{bmatrix}c & -s\\ s & c\end{bmatrix} = \begin{bmatrix}\bar{\sigma} & x\\ 0 & y\end{bmatrix}, \quad (18)$$

where $\delta_1 = \mathbf{R}^{(a)}(a,a)$, $\delta_2 = \mathbf{R}^{(a)}(b,b)$. If we take

$$c = \sqrt{\frac{\bar{\sigma}^2-\delta_2^2}{\delta_1^2-\delta_2^2}} \text{ and } s = \sqrt{1-c^2}, \quad (19)$$

we will get

$$x = \frac{sc(\delta_2^2-\delta_1^2)}{\bar{\sigma}} \text{ and } y = \frac{\delta_1\delta_2}{\bar{\sigma}}. \quad (20)$$

Let

$$\{\mathbf{G}_L^{(a)}\}^H = \bar{\sigma}^{-1}\begin{bmatrix}\mathbf{I}_{(a-1)} & & 0\\ & \begin{matrix}c\delta_1 & s\delta_2\\ -s\delta_2 & c\delta_1\end{matrix} & \\ 0 & & \mathbf{I}_{(U-a-1)}\end{bmatrix}, \quad (21)$$

$$\left\{\mathbf{M}^{(a)}\right\}^H\mathbf{R}^{(a)}\mathbf{M}^{(a)} = \begin{bmatrix}\bar{\sigma} & * & * & * & * & *\\ & \ddots & * & * & * & *\\ & & \delta_1 & 0 & * & *\\ & & 0 & \delta_2 & * & *\\ & & & & \ddots & *\\ & & & & & *\end{bmatrix}, \quad (22)$$

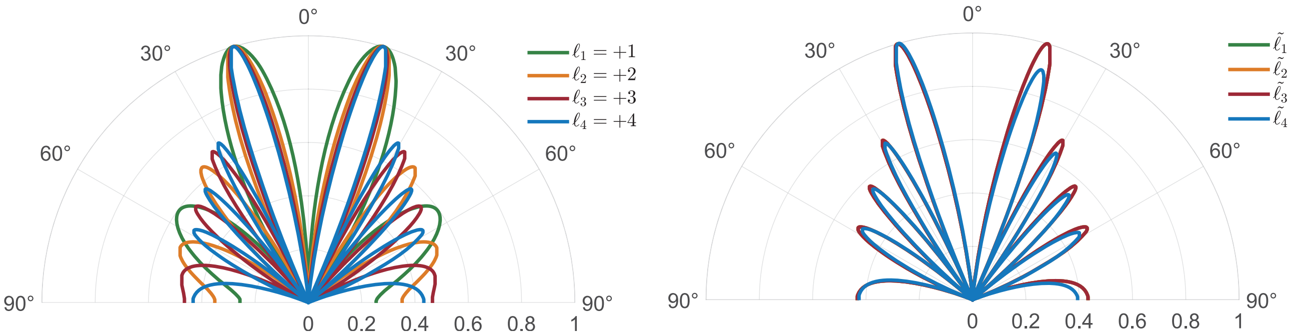

(a) (b)

FIGURE 5. The beam radiation patterns generated by: (a) the UCCA scheme proposed in [21], (b) the proposed NO-OAM scheme at 9GHz, $R_t = R_r = 3\lambda$.

$$\mathbf{G}_R^{(a)} = \begin{bmatrix} \mathbf{I}_{(a-1)} & & 0 \\ & \begin{matrix} c & -s \\ s & c \end{matrix} & \\ 0 & & \mathbf{I}_{(U-a-1)} \end{bmatrix}, \tag{23}$$

$$\mathbf{R}^{(a+1)} = \begin{bmatrix} \bar{\sigma} & * & * & * & * & * \\ & \ddots & * & * & * & * \\ & & \bar{\sigma} & x & * & * \\ & & 0 & y & * & * \\ & & & & \ddots & * \\ & & & & & * \end{bmatrix}, \tag{24}$$

then

$$\left(\left\{\mathbf{G}_L^{(a)}\right\}^H\right)\left(\left\{\mathbf{M}^{(a)}\right\}^H \mathbf{R}^{(a)}\mathbf{M}^{(a)}\right)\left(\mathbf{G}_R^{(a)}\right) = \left(\mathbf{R}^{(a+1)}\right). \tag{25}$$

- Step 4: Update $a = a + 1$ and go back to step2, until $a = U - 1$.

Because $\mathbf{M}^{(a)}$, $\mathbf{G}_L^{(a)}$ and $\mathbf{G}_R^{(a)}$ are all unitary matrices, we can set

$$\mathbf{S}_L = \mathbf{M}^{(1)}\mathbf{G}_L^{(1)}\mathbf{M}^{(2)}\mathbf{G}_L^{(2)}\cdots\mathbf{M}^{(U-1)}\mathbf{G}_L^{(U-1)}, \tag{26}$$

$$\mathbf{S}_R = \mathbf{M}^{(1)}\mathbf{G}_R^{(1)}\mathbf{M}^{(2)}\mathbf{G}_R^{(2)}\cdots\mathbf{M}^{(U-1)}\mathbf{G}_R^{(U-1)}. \tag{27}$$

Thus,

$$\mathbf{R} = \mathbf{S}_L^H\mathbf{W}\mathbf{S}_R. \tag{28}$$

That is $\mathbf{W} = \mathbf{S}_L\mathbf{R}\mathbf{S}_R^H$. Hence, $\Lambda_U = \mathbf{W}\mathbf{V} = \mathbf{S}_L\mathbf{R}\mathbf{S}_R^H\mathbf{V}$. ■

Now, we can design NO-OAM generation matrix as $\mathbf{P} = \mathbf{V}^H\mathbf{S}_R$ and let the post-processing matrix at the receiver be $\mathbf{S}_L^H\mathbf{F}_U$. From (12), we know that once R_t, R_r and λ are given, $\mathbf{P}$ and $\mathbf{S}_L^H\mathbf{F}_U$ can be completed characterized by D, which is much easier than estimating the whole channel matrix $\mathbf{H}$ in MIMO systems. Given $N = 8$, $\lambda = 0.033m$, $R_t = 3\lambda$, $R_r = 3\lambda$, D=50m, the generated phases of the NO-OAM beams with $\mathbf{P}$ are shown in Fig. 2 (e)–(h), where (e) $\tilde{\ell}_1 = 0.0159e^{j0.0377}\ell_1 + 0.9999e^{-j3.1036}\ell_4$, (f) $\tilde{\ell}_2 = 0.6730e^{-j3.1039}\ell_1 + 0.7395e^{-j1.5330}\ell_2 + 0.0107e^{-j3.1036}\ell_4$, (g) $\tilde{\ell}_3 = 0.5659e^{j0.0377}\ell_1 + 0.5152e^{-j1.5330}\ell_2 + 0.6436e^{-j1.5330}\ell_3 + 0.0090e^{j0.0380}\ell_4$, (h) $\tilde{\ell}_4 = 0.4759e^{-j3.1039}\ell_1 + 0.4332e^{j1.6086}\ell_2 + 0.7654e^{-j1.5330}\ell_3 + 0.0075e^{-j3.1036}\ell_4$; $\ell_1 = 0$, $\ell_2 = +1$, $\ell_3 = -1$, $\ell_4 = +2$. In addition, the beam radiation patterns generated by the orthogonal OAM scheme and the proposed NO-OAM scheme are compared in Fig. 3. It can been seen clearly from the figure that the proposed method regulates the beam divergence angles of all NO-OAM modes to be the same with only one UCA, thus circumventing the problem of different OAM modes having large different receive SNRs at the receive UCA with a fixed aperture.

Algorithm 1 Successive Interference Cancellation

Input: $\mathbf{R} \in \mathbb{R}^{N\times N}$: the effective channel matrix, $\mathbf{x}' \in \mathbb{R}^{N\times 1}$: the received signal after post-processing
Output: $\mathbf{x}^* \in \mathbb{R}^{N\times 1}$

```
procedure SIC(R, x')
    x* ← 0
for i = N; i ≥ 1; i − − do
    sum ← 0
    for j = 1; j ≤ N; j + + do
        sum ← sum + R(i, j) * x*(j)
        x*(i) ← (x'(i) − sum) / R(i, i)
        x*(i) ← Q(x*(i)) : Q(·) maps the complex signal to a point in the constellation diagram.
    end
end
end procedure
```

B. MULTIPLEXING AND RECEPTION OF NO-OAM SIGNALS

According to the above design, the generation, transmission and reception of NO-OAM signals could be formulated by $\mathbf{F}_U^H\mathbf{P}$ and $\mathbf{S}_L^H\mathbf{F}_U$ as the precoding matrix and the detection matrix, respectively, which can be expressed as

$$\begin{aligned} \mathbf{x}' &= \mathbf{S}_L^H\mathbf{F}_U\left(\mathbf{H}\mathbf{F}_U^H\mathbf{P}\mathbf{x} + \mathbf{z}\right) \\ &= \mathbf{R}\mathbf{x} + \bar{\mathbf{z}}, \end{aligned} \tag{29}$$

where $\mathbf{R}$ is the effective NO-OAM channel, and $\bar{\mathbf{z}} = (\mathbf{S}_L^H\mathbf{F}_U)\mathbf{z}$ is the noise. The proposed NO-OAM communication framework including the generation, multiplexing and

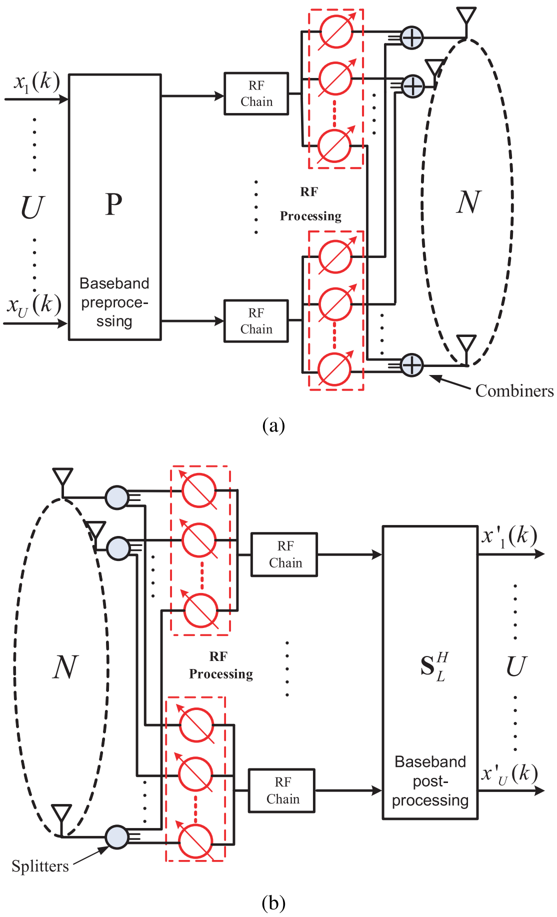

FIGURE 6. The simplified implementation structures of UCA-based NO-OAM (a) transmitter, and (b) receiver.

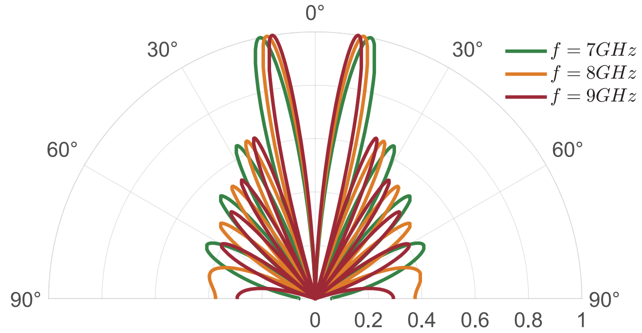

FIGURE 7. Beam radiation patterns generated by NO-OAM with different carrier frequencies, $R_t = R_r = 0.1$m.

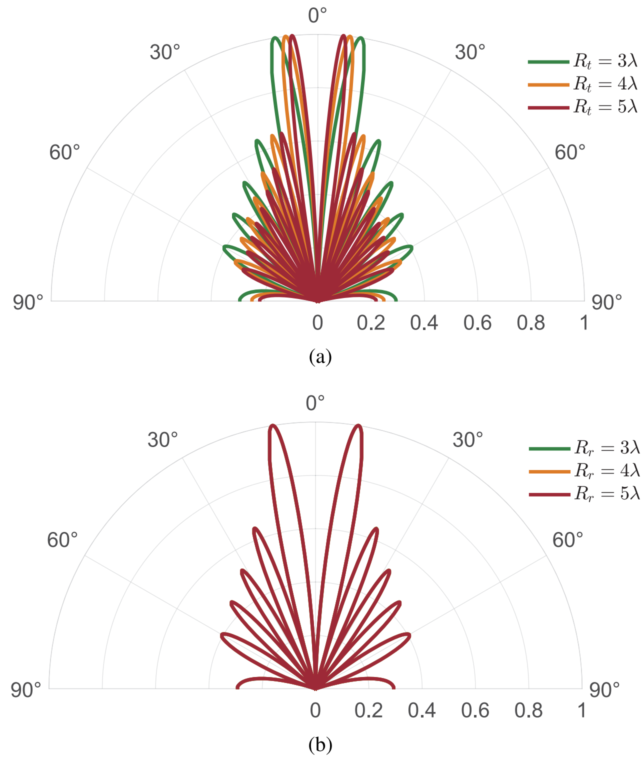

FIGURE 8. Beam radiation patterns generated by NO-OAM with different: (a) $R_t(R_r = 3\lambda)$, (b) $R_r(R_t = 3\lambda)$ at 9GHz.

reception of NO-OAM signals is shown in Fig. 6, in which the phase shifters network (PSN) and power combiners at the transmitter are used for generating and multiplexing orthogonal OAM beams, PSN and power splitters at the receiver enable the de-multiplexing and reception of multi-stream OAM signals [14], and $\mathbf{P}$ and $\mathbf{S}_L^H$ are operated in baseband processing. Due to $\mathbf{R}$ being upper triangular rather than diagonal in (9), it results in the sub-channels no longer orthogonal. Hence, the receiver has to detect the signals through SIC technology. Because only the diagonal element of the Uth row of $\mathbf{R}$ is nonzero, there is no interference from other sub-channels. We first solve the Uth signal, and then bring it back into the $(U-1)$ row to eliminate the interference it brings, and solve the $(U-1)$th signal. After U iterations, we solve all the U received signals. The implementation steps of SIC in specified in **Algorithm 1**.

Since the SIC eliminates the non-diagonal elements of $\mathbf{R}$, the channel capacity of the NO-OAM multiplexing system is

$$C_{\text{NO-OAM}} = U \log_2\left(1 + \frac{\rho}{U}\bar{\sigma}^2\right). \tag{30}$$

Through a simple proof with mean value inequality, we can obtain

$$\lim_{\rho\to\infty} C_{\text{OAM}} - C_{\text{NO-OAM}} = \lim_{\rho\to\infty} \log_2 \frac{\prod_{u=1}^{U}\left(U+\rho\lambda_u^2\right)}{\left(U+\rho\bar{\sigma}^2\right)^U} = 0, \tag{31}$$

which reveals the channel capacity of the proposed NO-OAM multi-mode multiplexing scheme being asymptotically equivalent with traditional orthogonal OAM multi-mode multiplexing.

V. NUMERICAL SIMULATIONS AND RESULTS

In this section, we show the performances of the proposed NO-OAM multi-mode multiplexing scheme by numerical simulations. First, we investigate the performance of the beam divergence angle adjustment of the NO-OAM scheme.

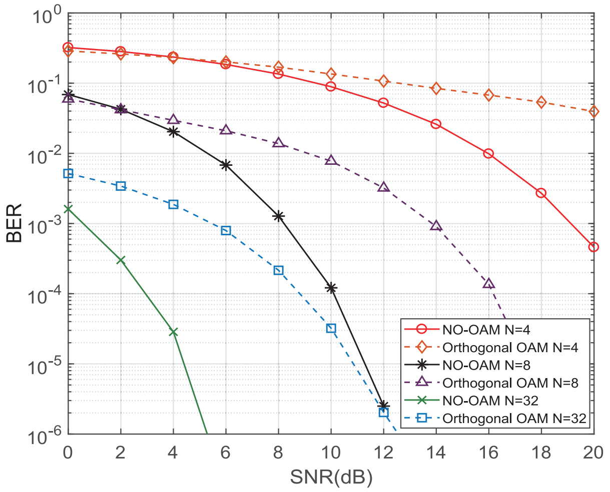

FIGURE 9. BER performances of NO-OAM and traditional OAM.

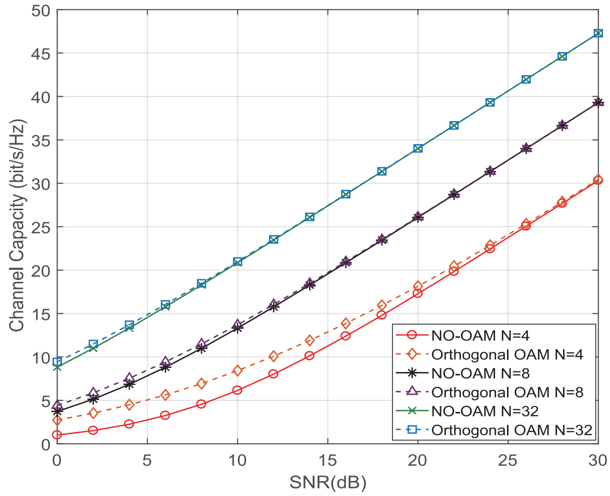

FIGURE 10. Channel capacity of NO-OAM and traditional OAM.

TABLE 1. Beam adjustment comparison between UCCA [21] and the proposed NO-OAM for a fixed divergence angle.

	NO-OAM	UCCA [21]
Number of UCAs	1	4
Divergence angle(°)	16.4	16.4
Mainlobe width(rad)	0.043π	0.096π
PSLR(dB)	-1.69	-1.63

We mainly focus on the four metrics: divergence angle, minimum number of UCAs, mainlobe width and peak sidelobe rate (PSLR). In Fig. 7 and Fig. 8, we verify the effects of the carrier frequency, R_t and R_r on the beam divergence angle. It can be seen from the figures that the larger the R_t or the higher the carrier frequency is, the smaller the divergence angle becomes, however, the divergence angle does not change with R_r.

The four metrics comparison between the UCCA scheme [21] and our proposed NO-OAM scheme, which has been illustrated in Fig. 5, are quantitatively listed in the Table 1. For fair comparison, the divergence angles of both schemes are adjusted to the same 16.4°. We observe that the 3-dB mainlobe width of the beam generated by the NO-OAM scheme is smaller than that of the UCCA scheme, which means that the beam directivity of the NO-OAM scheme is better. The PSLR values of the two schemes are close. It is worth noting that the UCCA scheme requires U UCAs with different radii, while the NO-OAM scheme only requires 1 UCA. It follows that the NO-OAM scheme can reduce the hardware cost and take full use of spatial degrees of freedom.

Then, we verify the BER and channel capacity performances of the proposed NO-OAM scheme through comparing with traditional orthogonal OAM scheme. In the simulation, $N = 4, 8, 32$, $U = 4$, ($\ell_1 = 0$, $\ell_2 = +1$, $\ell_3 = -1$, $\ell_4 = +2$), and QPSK is adopted for modulation. In Fig. 9, the BER performances of the two schemes are compared. It can be seen from the figure that the BER of the NO-OAM scheme is much lower than that of the traditional orthogonal OAM. The results coincide with the previous theoretical analysis. The NO-OAM equalizes the power of all OAM beams thus improving the SNR of the worst channel of the traditional orthogonal OAM, which is reflected by the phenomenon that the divergence angles of all the OAM beams being regulated. Thus, the improvement of SNRs of the worst channels greatly enhance the system BER performance. In Fig. 10, the channel capacity performances of the two schemes are compared. When N is small and the SNR is in low regime, the channel capacity of NO-OAM system is lower than that of the traditional orthogonal OAM system. As the SNR and N increase, the gap between the two schemes is vanishing small, which coincides with our previous theoretical analysis in (31) as well.

VI. CONCLUSION

In this article, we propose a NO-OAM multi-mode multiplexing scheme based on UCAs, which includes the generation, multiplexing transmission and reception of non-orthogonal OAM modes. The proposed generation method regulates the beam divergence angles of all non-orthogonal OAM modes to be the same with only one UCA, circumventing the problem of different OAM modes having large different receive SNRs. As the sacrifice, the transmitter requires the knowledge of distance information to generate the NO-OAM beams and the receiver has to utilize SIC to cancel the inter-mode interference. Mathematical analysis and numerical simulations show that the proposed NO-OAM scheme has slightly better beam adjustment effect and lower hardware cost than the UCCA beam adjustment scheme, and has asymptotically equivalent channel capacity and much lower BER in contrast to the traditional orthogonal OAM multi-mode transmission. The proposed NO-OAM multi-mode multiplexing scheme provides another novel idea for OAM multi-mode multiplexing.

ACKNOWLEDGMENT

The authors would like to thank the Editor and the anonymous reviewers for their careful reading and valuable suggestions that helped to improve the quality of this manuscript.

REFERENCES

[1] (Sep. 2018). *World Radiocommunication Conference (WRC)*. [Online]. Available: https://www.itu.int/en/ITU-R/conferences/wrc/Pages/default.aspx
[2] L. Allen, M. W. Beijersbergen, R. J. C. Spreeuw, and J. P. Woerdman, "Orbital angular momentum of light and the transformation of Laguerre-Gaussian laser modes," *Phys. Rev. A*, vol. 45, no. 11, pp. 8185–8189, 1992.
[3] S. M. Mohammadi *et al.*, "Orbital angular momentum in radio—A system study," *IEEE Trans. Antennas Propag.*, vol. 58, no. 2, pp. 565–572, Feb. 2010.
[4] F. Tamburini, E. Mari, T. Bo, C. Barbieri, and F. Romanato, "Experimental verification of photon angular momentum and vorticity with radio techniques," *Appl. Phys. Lett.*, vol. 99, no. 20, 2011, Art. no. 204102.
[5] A. Tennant and B. Allen, "Generation of radio frequency OAM radiation modes using circular time-switched and phased array antennas," in *Proc. Loughborough Antennas Propag. Conf. (LAPC)*, Nov. 2012, pp. 1–4.
[6] F. E. Mahmouli and S. Walker, "Orbital angular momentum generation in a 60GHz wireless radio channel," in *Proc. 20th Telecommun. Forum (TELFOR)*, Nov. 2012, pp. 315–318.
[7] O. Edfors and A. J. Johansson, "Is orbital angular momentum (OAM) based radio communication an unexploited area?" *IEEE Trans. Antennas Propag.*, vol. 60, no. 2, pp. 1126–1131, Feb. 2012.
[8] Y. Yan *et al.*, "High-capacity millimetre-wave communications with orbital angular momentum multiplexing," *Nat. Commun.*, vol. 5, p. 4876, Sep. 2014.
[9] R. Gaffoglio, A. Cagliero, A. De Vita, and B. Sacco, "OAM multiple transmission using uniform circular arrays: Numerical modeling and experimental verification with two digital television signals," *Radio Sci.*, vol. 51, no. 6, pp. 645–658, 2016.
[10] X. Ge, R. Zi, X. Xiong, Q. Li, and L. Wang, "Millimeter wave communications with OAM-SM scheme for future mobile networks," *IEEE J. Sel. Areas Commun.*, vol. 35, no. 9, pp. 2163–2177, Sep. 2017.
[11] Y. Ren *et al.*, "Line-of-sight millimeter-wave communications using orbital angular momentum multiplexing combined with conventional spatial multiplexing," *IEEE Trans. Wireless Commun.*, vol. 16, no. 5, pp. 3151–3161, May 2017.
[12] W. Zhang *et al.*, "Mode division multiplexing communication using microwave orbital angular momentum: An experimental study," *IEEE Trans. Wireless Commun.*, vol. 16, no. 2, pp. 1308–1318, Feb. 2017.
[13] D. Lee *et al.*, "An experimental demonstration of 28 GHz band wireless OAM-MIMO (orbital angular momentum multi-input and multi-output) multiplexing," in *Proc. IEEE 87th Veh. Technol. Conf.*, 2018, pp. 1–5.
[14] R. Chen, W. Yang, H. Xu, and J. Li, "A 2-D FFT-based transceiver architecture for OAM-OFDM systems with UCA antennas," *IEEE Trans. Veh. Technol.*, vol. 67, no. 6, pp. 5481–5485, Jun. 2018.
[15] R. Chen, H. Xu, X. Wang, and J. Li, "On the performance of OAM in keyhole channels," *IEEE Wireless Commun. Lett.*, vol. 8, no. 1, pp. 313–316, Feb. 2019.
[16] C. Zhang and Y. Zhao, "Orbital angular momentum nondegenerate index mapping for long distance transmission," *IEEE Trans. Wireless Commun.*, vol. 18, no. 11, pp. 5027–5036, Nov. 2019.
[17] W. Cheng, W. Zhang, H. Jing, S. Gao, and H. Zhang, "Orbital angular momentum for wireless communications," *IEEE Wireless Commun.*, vol. 26, no. 1, pp. 100–107, Feb. 2019.
[18] R. Chen, H. Zhou, M. Moretti, X. Wang, and J. Li, "Orbital angular momentum waves: Generation, detection, and emerging applications," *IEEE Commun. Surveys Tuts.*, vol. 22, no. 2, pp. 840–868, 2nd Quart., 2020.
[19] R. Chen, W.-X. Long, X. Wang, and J. Li, "Multi-mode OAM radio waves: Generation, angle of arrival estimation and reception with UCAs," *IEEE Trans. Wireless Commun.*, vol. 19, no. 10, pp. 6932–6947, Oct. 2020.
[20] R. Chen, M. Zou, X. Wang, and A. Tennant, "Generation and beam steering of arbitrary-order OAM with time-modulated circular arrays," *IEEE Syst. J.*, early access, Sep. 7, 2020, doi: 10.1109/JSYST.2020.3019337.
[21] T. Yuan, H. Wang, Y. Qin, and Y. Cheng, "Electromagnetic vortex imaging using uniform concentric circular arrays," *IEEE Antennas Wireless Propag. Lett.*, vol. 15, pp. 1024–1027, Mar. 2016.
[22] R. Chen, H. Xu, M. Moretti, and J. Li, "Beam steering for the misalignment in UCA-based OAM communication systems," *IEEE Wireless Commun. Lett.*, vol. 7, no. 4, pp. 582–585, Aug. 2018.
[23] Y. Jiang, W. W. Hager, and J. Li, "The geometric mean decomposition," *Linear Algebra Appl.*, vol. 396, pp. 373–384, Feb. 2005.

RUI CHEN (Member, IEEE) received the B.S., M.S., and Ph.D. degrees in communications and information systems from Xidian University, Xi'an, China, in 2005, 2007, and 2011, respectively. From 2014 to 2015, he was a Visiting Scholar with Columbia University, New York. He is currently an Associate Professor and a Ph.D. supervisor with the State Key Lab of ISN and School of Telecommunications Engineering, Xidian University. He has published about 60 papers in international journals and conferences and held 20 patents. His research interests include broadband wireless communication systems, array signal processing, and intelligent transportation systems. He is an Associate Editor for *International Journal of Electronics, Communications, and Measurement Engineering* (IGI Global).

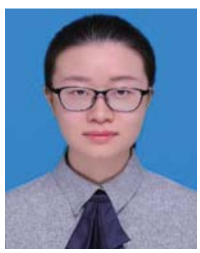

RUNZHONG YAO (Graduate Student Member, IEEE) received the B.S. degree in telecommunication engineering from Xidian University, Xi'an, China, in 2019, where she is currently pursuing the M.S. degree in communications and information systems. Her current research interests include broadband wireless communication systems and antenna array design.

WEN-XUAN LONG (Graduate Student Member, IEEE) received the B.S. degree (with Highest Hons.) in rail transit signal and control from Dalian Jiaotong University, Dalian, China, in 2017. She is currently pursuing the double Ph.D. degrees in communications and information systems with Xidian University, China, and University of Pisa, Italy. Her research interests include broadband wireless communication systems and array signal processing.

MARCO MORETTI (Member, IEEE) received the degree in electronic engineering from the University of Florence, Florence, Italy, in 1995, and the Ph.D. degree from the Delft University of Technology, Delft, The Netherlands, in 2000. From 2000 to 2003, he was a Senior Researcher with Marconi Mobile. He is currently an Associate Professor with the University of Pisa, Pisa, Italy. His research interests include resource allocation for multicarrier systems, synchronization, and channel estimation. He is currently an Associate Editor of the IEEE TRANSACTIONS ON SIGNAL PROCESSING.

JIANDONG LI (Fellow, IEEE) received the B.E., M.S., and Ph.D. degrees in communications engineering from Xidian University, Xi'an, China, in 1982, 1985, and 1991, respectively. He was a Visiting Professor with the Department of Electrical and Computer Engineering, Cornell University from 2002 to 2003. He has been a Faculty Member with the School of Telecommunications Engineering, Xidian University, since 1985, where he is currently a Professor and the Vice Director of the Academic Committee, State Key Laboratory of Integrated Service Networks. His major research interests include wireless communication theory, cognitive radio, and signal processing. He was recognized as a Distinguished Young Researcher by NSFC and a Changjiang Scholar by the Ministry of Education, China, respectively. He served as the General Vice Chair of ChinaCom in 2009 and the TPC Chair of the IEEE ICCC in 2013.